

Two-dimensional horizontal visibility graph analysis of human brain aging on gray matter

Huang-Jing Ni(倪黄晶), Ruo-Yu Du(杜若瑜), Lei Liang(梁磊), Ling-Ling Hua(花玲玲), Li-Hua Zhu(朱丽华), and Jiao-Long Qin(秦姣龙)

Citation: Chin. Phys. B, 2023, 32 (**7**): 078501. DOI: 10.1088/1674-1056/acc7f7
Journal homepage: http://cpb.iphy.ac.cn; http://iopscience.iop.org/cpb

What follows is a list of articles you may be interested in

Enhancing convolutional neural network scheme forrheumatoid arthritis grading with limited clinical data

Jian Tang(汤键), Zhibin Jin(金志斌), Xue Zhou(周雪), Weijing Zhang(张玮婧), Min Wu(吴敏), Qinghong Shen(沈庆宏), Qian Cheng(程茜), Xueding Wang(王学鼎), Jie Yuan(袁杰)
Chin. Phys. B, 2019, 28 (**3**): 038701. DOI: 10.1088/1674-1056/28/3/038701

Shifting curves based on the detector integration effect for x-ray phase contrast imaging

Jun Yang(杨君), Jin-Chuan Guo(郭金川), Yao-Hu Lei(雷耀虎), Ming-Hao Yi(易明皓), Li Chen(陈力)
Chin. Phys. B, 2017, 26 (**2**): 028701. DOI: 10.1088/1674-1056/26/2/028701

Nonlinear profile order for three-dimensional hybrid radial acquisition applied to self-gated free-breathing cardiac cine MRI

Yanchun Zhu(朱艳春), Pascal Spincemaille, Jing Liu(刘静), Shuo Li(李硕), Thanh D Nguyen, Martin R Prince, Yaoqin Xie(谢耀钦), Yi Wang(王乙)
Chin. Phys. B, 2017, 26 (**1**): 018701. DOI: 10.1088/1674-1056/26/1/018701

Simple phase extraction in x-ray differential phase contrast imaging

Xin Liu(刘鑫), Jin-Chuan Guo(郭金川), Yao-Hu Lei(雷耀虎), Ji Li(李冀), Han-Ben Niu(牛憨笨)
Chin. Phys. B, 2016, 25 (**2**): 028704. DOI: 10.1088/1674-1056/25/2/028704

Experimental investigations of the functional morphology of dragonfly wings

H. Rajabi, A. Darvizeh
Chin. Phys. B, 2013, 22 (**8**): 088702. DOI: 10.1088/1674-1056/22/8/088702

Two-dimensional horizontal visibility graph analysis of human brain aging on gray matter

Huang-Jing Ni(倪黄晶)[1,2], Ruo-Yu Du(杜若瑜)[1,2], Lei Liang(梁磊)[1], Ling-Ling Hua(花玲玲)[3], Li-Hua Zhu(朱丽华)[4], and Jiao-Long Qin(秦姣龙)[5,†]

[1] *School of Geographic and Biologic Information, Nanjing University of Posts and Telecommunications, Nanjing* 210003, *China*
[2] *Smart Health Big Data Analysis and Location Services Engineering Laboratory of Jiangsu Province, Nanjing* 210003, *China*
[3] *Department of Psychiatry, the Affiliated Brain Hospital of Nanjing Medical University, Nanjing* 210029, *China*
[4] *Jiangsu Health Vocational College, Nanjing* 211800, *China*
[5] *School of Computer Science and Engineering, Nanjing University of Science and Technology, Nanjing* 210094, *China*

(Received 11 November 2022; revised manuscript received 14 January 2023; accepted manuscript online 28 March 2023)

Characterizing the trajectory of the healthy aging brain and exploring age-related structural changes in the brain can help deepen our understanding of the mechanism of brain aging. Currently, most structural magnetic resonance imaging literature explores brain aging merely from the perspective of morphological features, which cannot fully utilize the gray-scale values containing important intrinsic information about brain structure. In this study, we propose the construction of two-dimensional horizontal visibility graphs based on the pixel intensity values of the gray matter slices directly. Normalized network structure entropy (NNSE) is then introduced to quantify the overall heterogeneities of these graphs. The results demonstrate a decrease in the NNSEs of gray matter with age. Compared with the middle-aged and the elderly, the larger values of the NNSE in the younger group may indicate more homogeneous network structures, smaller differences in importance between nodes and thus a more powerful ability to tolerate intrusion. In addition, the hub nodes of different adult age groups are primarily located in the precuneus, cingulate gyrus, superior temporal gyrus, inferior temporal gyrus, parahippocampal gyrus, insula, precentral gyrus and postcentral gyrus. Our study can provide a new perspective for understanding and exploring the structural mechanism of brain aging.

Keywords: two-dimensional horizontal visibility graph, brain aging, structural magnetic resonance imaging, network structure entropy

PACS: 87.18.–h, 87.57.–s, 87.61.–c, 87.85.D– **DOI:** 10.1088/1674-1056/acc7f7

1. Introduction

Functional decline is a time-dependent phenomenon associated with aging. During normal aging, the brain changes due to cell growth, myelination and atrophy as part of both progressive and degenerative processes.[1] Brain aging will not only affect the individual's coordination, language, emotional control and cognitive abilities, and other functions,[2] but also may increase the incidence of age-related diseases such as dementia and stroke. As a result, adverse effects will significantly reduce the quality of life of individuals and bring a significant burden to society. Characterizing the trajectory of the healthy aging brain and exploring age-related structural changes in the brain can help deepen our understanding of the mechanism of brain aging and thus promote early prevention of and intervention in diseases related to brain aging.[3]

Previous structural magnetic resonance imaging (sMRI) research has shown that gray matter and white matter will atrophy during brain aging, accompanied by reduced gray matter volume, narrowed gyri and enlarged sulci.[4,5] According to studies of brain volume, cortical thickness and magnetization transfer concentration, the human brain follows specific patterns during normal aging.[4,6,7] For instance, Bethlehem *et al.*[4] revealed that the total volume of cortical gray matter increased strongly after mid-gestation, peaked at about 6 years and then followed a linear decrease. Additionally, the total volume of white matter increased rapidly from mid-gestation to early childhood, peaking at 28.7 years and beginning to decline after 50 years. Karolis *et al.*[7] found that the white matter magnetization transfer concentration decreased from anterior to posterior with brain aging. In the lateral white matter region, magnetization transfer concentration increased before 45 years of age and then moderately reduced thereafter. These studies explored the normal aging pattern of the human brain from the perspective of brain morphology. Turning now to the sMRI data *per se*, in addition to characterizing the morphology of each brain tissue it can also provide the gray value information for each voxel. Existing evidence has indicated that the intensity of the texture signal of gray value in sMRI is not uniform and has its own fluctuations.[8,9] Accordingly, the gray values of sMRI data also reveal important information about the structure of the human brain. In this regard, exploring sMRI signal intensity can provide a new perspective for studying brain aging, and such studies are currently limited.

The popular two-dimensional visibility graph (2DVG)

†Corresponding author. E-mail: jiaolongq@njust.edu.cn
© 2023 Chinese Physical Society and IOP Publishing Ltd

method can perform network conversion directly on gray values. In addition to the ability to extract rich features from graphs, 2DVG has good computational efficiency, which is suitable for image processing and image classification.[10] It has been successfully used in a wide range of image-processing applications. For example, Iacovacci *et al.*[10] used 2DVGs as image filters in material texture detection to extract features and perform multi-class image classification, achieving accuracies of over 95%. Nowak *et al.*[11] adopted the 2DVG algorithm to accurately quantify cell protrusions and invaginations in leaf epidermis, exhibiting its advantages by comparing different shapes, describing key features and characterizing cell shape complexity simultaneously. Moreover, Xiao *et al.*[12] revealed that the 2DVG algorithm could be used to detect the pattern-related new features of two-dimensional landscapes. These studies have demonstrated the effectiveness of the 2DVG algorithm in natural image texture analysis. However, whether this algorithm can be applied to medical image texture analysis, such as sMRI images, is still unclear. According to the different visibility angles allowed between two points, the constructed visibility graph can be either a natural visibility graph or a horizontal visibility graph (HVG). In contrast to the natural visibility graph, the HVG has fewer statistics and more straightforward geometrical visibility criteria.[13] Therefore, we constructed two-dimensional HVGs (2DHVGs) based on the pixel intensity values of the gray matter slices directly and then introduced the normalized network structure entropy to characterize the trajectory pattern of brain aging, which could be helpful for understanding how the brain ages.

2. Materials and methods

2.1. Materials and data preprocessing

The T1-weighted sMRI data were downloaded from the available Southwest University adult lifespan dataset.[14] This study analyzed 494 healthy adults (187 men and 307 women, aged 19 to 80 years). The subjects aged 19 to 25 years were college students at Southwest University, whereas those aged 26 to 40 years were staff members at Southwest University, with the rest having been recruited from communities near the university campus. All the included participants were free of psychiatric and neurological disorders and had no metal implants in their brains. Additionally, all participants were required to have no brain trauma, taken no psychoactive drugs within the previous 3 months and had no alcohol before the scan. During the scan, all subjects were required to lie still, close their eyes, refrain from thinking and stay awake. Dataset collection was approved by the Research Ethics Committee of the Brain Imaging Center at Southwestern University, and written informed consent was collected before data acquisition. The work by Wei *et al.*[14] gives more details about the dataset.

To obtain high-resolution T1-weighted anatomical images, a magnetization-prepared rapid gradient echo sequence was used with the following parameters: repetition time 1900 ms, echo time 2.52 ms, inversion time 900 ms, flip angle 90°, resolution matrix 256×256, number of slices 176, thickness 1.0 mm and voxel size 1 mm×1 mm×1 mm.

Standard preprocessing of sMRI data was performed in SPM12 software.[15] After manual reorientation and skull-stripping, spatial normalization to the MNI space and segmentation steps were conducted. Specifically, diffeomorphic anatomical registration using the exponentiated Lie algebra strategy[16] was adopted in this study to obtain the segmented gray matter, white matter and cerebrospinal fluid with high quality. During this step, the structural images were resampled at a voxel size of 1.5 mm isotropic. As a final step, the sMRI signal intensities were normalized and converted into 255 gray scale values to eliminate the possible adverse effects of different intensity ranges among subjects. After preprocessing, further analysis was conducted on the segmented and converted gray matter.

2.2. The construction of a 2DHVG

In the one-dimensional HVG algorithm proposed by Luque *et al.*,[13] each data point in the time series corresponds to a node in the mapped network. The link between data points should satisfy the following visibility criteria: for any two points (t_a, y_a) and (t_b, y_b) in the time series, if any arbitrary point (t_c, y_c) between them satisfies $y_c < \min\{y_a, y_b\}, \forall t_c : t_a < t_c < t_b$, these two points are defined as visible to each other.

A 2DHVG[10] can be constructed by generalizing the construction concept of a HVG from one dimension to two dimensions. Specifically, let an image I be a matrix where I_{ij} ($I_{ij} \in R$) is the pixel value at row i and column j. Take each pixel in the two-dimensional image as a network node, and its corresponding pixel's gray value determines each node's height. For each node, its connections with other nodes can be evaluated in four directions, i.e., upper and lower, left and right, diagonal, anti-diagonal. The relationships between nodes in each direction are then judged using the visibility criterion of one-dimensional HVG. Mathematically, two nodes ij and $i'j'$ are linked if (1) $(i = i') \vee (j = j') \vee [(i = i' + p) \wedge (j = j' + p)]$, for some integer p, and (2) in the ordered sequence that includes ij and $i'j'$, I_{ij} and $I_{i'j'}$ are connected to each other in the HVG. An illustrative example of the construction of a 2DHVG is given in Fig. 1. The 2DHVG on the image can finally be constructed by traversing all nodes.

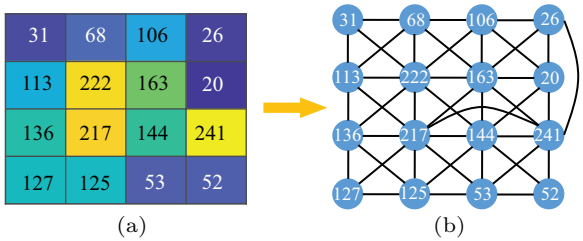


Fig. 1. Construction diagram of a two-dimensional horizontal visibility graph (2DHVG). (a) Example of an image matrix. (b) The constructed 2DHVG. Each numerical value represents the gray value in the corresponding pixel as a node.

2.3. Extraction of the normalized network structure entropy

In order to measure the topological heterogeneity of the 2DHVG, the network structure entropy (NSE)[17] is used in this study. Given a network of N nodes, letting k_i be the degree of node v_i, the importance of the node v_i can be measured by $I_i = k_i / \sum_{j=1}^{N} k_j$. Accordingly, the NSE can be defined as $\mathrm{NSE} = -\sum_{i=1}^{N} I_i \times \ln I_i$. As for the nodes with $k_i = 0$, it is specified that $0 \times \ln 0 = 0$. For a totally homogeneous network (i.e., $k_1 = k_2 = \cdots = k_N$), the importance of each node is equal and can be expressed by $I_i = 1/N$. In this case, $\mathrm{NSE}_{\max} = \ln N$. Conversely, in a star-like network, all nodes are connected only to the central node ($k_i = N-1$ and $k_j = 1, \forall j \neq i$). The minimum of NSE can be obtained by $\mathrm{NSE}_{\min} = \ln[4(N-1)]/2$ for this most heterogeneous network. Additionally, in order to eliminate the effect of the number of nodes, we further normalized the NSE (NNSE) as follows:

$$\begin{aligned} \mathrm{NNSE} &= \frac{\mathrm{NSE} - \mathrm{NSE}_{\min}}{\mathrm{NSE}_{\max} - \mathrm{NSE}_{\min}} \\ &= \frac{-2\sum_{i=1}^{N} I_i \times \ln I_i - \ln[4(N-1)]}{2\ln N - \ln[4(N-1)]}. \end{aligned} \tag{1}$$

3. Results

3.1. Construction results for 2DHVGs on gray matter slices

In this study, the preprocessed gray matter volumes were first resliced in the sagittal plane according to their original scanning direction. Subsequently, the 2DHVGs were constructed on every single slice for each subject. The illustrative construction results of 2DHVG on three typical gray matter slices are shown in Fig. 2. Even though the shapes of the constructed 2DHVGs on different slices differed, they were all centered at the hub nodes and diverged at the terminal nodes.

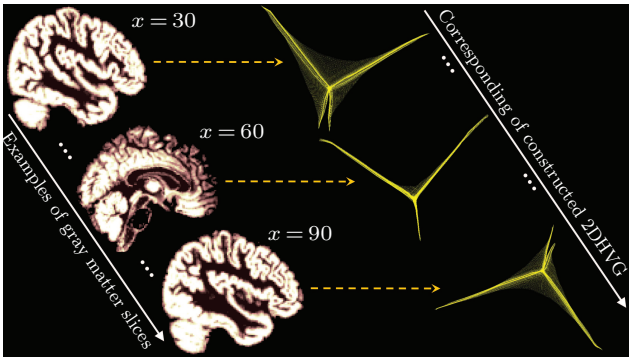


Fig. 2. The construction results of two-dimensional horizontal visibility graphs (2DHVGs) on three different gray matter slices ($x = 30$, 60 and 90) from the same subject.

3.2. Results of brain aging analysis on the NNSE

As a first step, we examined the degree distributions after constructing the 2DHVGs. The majority of nodes were connected only to their adjacent nodes on the upper and lower, left and right, diagonal, and anti-diagonal directions (i.e., degree ≤ 8), while only a few nodes had larger degrees. As shown in Fig. 3, the second half of the degree distribution (i.e., degree > 13) followed a power-law form, which suggested heterogeneity in the topology of 2DHVGs.

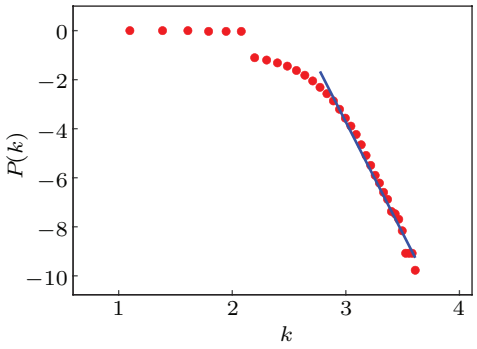


Fig. 3. The log–log degree distribution plot of the two-dimensional horizontal visibility graph on a gray matter slice. The abscissa represents the logarithm of the degree values, and the ordinate represents the logarithm of the cumulative degree distribution.

As a next step, we extracted the NNSE from the 2DHVG to measure its topological heterogeneity. After calculating the NNSEs of each gray matter slice of each subject, the NNSEs of all slices from the same subject were then averaged to obtain the final NNSE for this subject. All slices with a maximum degree of less than 10 were removed to reduce the impact of minor and unrelated brain tissues on the calculation results. Next, in order to explore the relationship between the NNSEs of gray matter and age, we further averaged the NNSEs from subjects with the same age and then conducted a correlation analysis. The results are shown in Fig. 4. Through quadratic polynomial nonlinear fitting, the NNSEs of the gray matter showed a decreasing trend with age ($R^2 = 0.45$, RMSE $= 0.0002$).

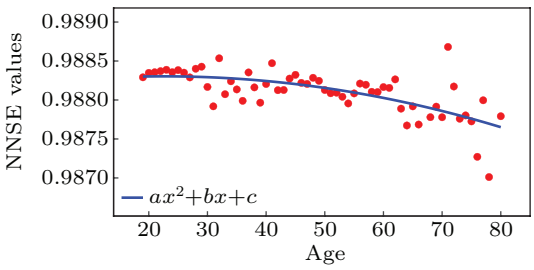


Fig. 4. Relationship between the normalized network structure entropy (NNSE) values of gray matter and age (in years). In the nonlinear fitting model (i.e., $Y = ax^2 + bx + c$) given in the legend, the parameters are calculated as $a = -1.98 \times 10^{-7}$, $b = 8.97 \times 10^{-6}$ and $c = 0.99$.

3.3. Hub node distribution in different age groups

Based on the 2DHVG constructed in each slice, the degree value of each pixel can be determined. The three-dimensional gray matter image reconstruction based on node degree values can thus be achieved by replacing gray values with degree values. Next, by setting 10 years as an age span, all subjects aged 20–79 years were divided into different age groups. In order to explore the distribution of hub nodes in different age groups, we accumulated and merged the three-dimensional brain data of degree values from subjects of the same age group, selecting those nodes with the top 20 largest degrees. In Fig. 5, we present the distribution of hub nodes and the participation ratios of their assigned brain networks for different age groups. As illustrated in Figs. 5(a)–5(c) and 5(g)–5(i), the common hub nodes in all age groups (aged 20–79 years) were identified in the right precuneus, bilateral anterior cingulate gyrus, bilateral middle cingulate gyrus, right posterior cingulate gyrus, left superior temporal gyrus and right insula. After assigning each hub node to the brain networks, the participation ratios for the involved brain networks can be obtained. As shown in Figs. 5(d)–5(f) and 5(j)–5(l), the greatest number of hub nodes were located in the saliency network (SAN) regardless of age group. Furthermore, the participation ratios of the SAN increased from early adulthood to adulthood, peaked at the age of 40–49 years and then decreased with age. Also, combinations of the SAN and the default mode network (DMN) consistently accounted for the overwhelming majority of brain networks. For younger and middle-aged groups (i.e., age ranges 20–29, 30–39, 40–49 and 50–59 years), combinations of SAN and DMN accounted for more than 90% of networks, while for the elderly (i.e., age ranges 60–69 and 70–79 years), it fell to about 80%. Additionally, the number of participating brain networks exhibited an increasing trend with aging.

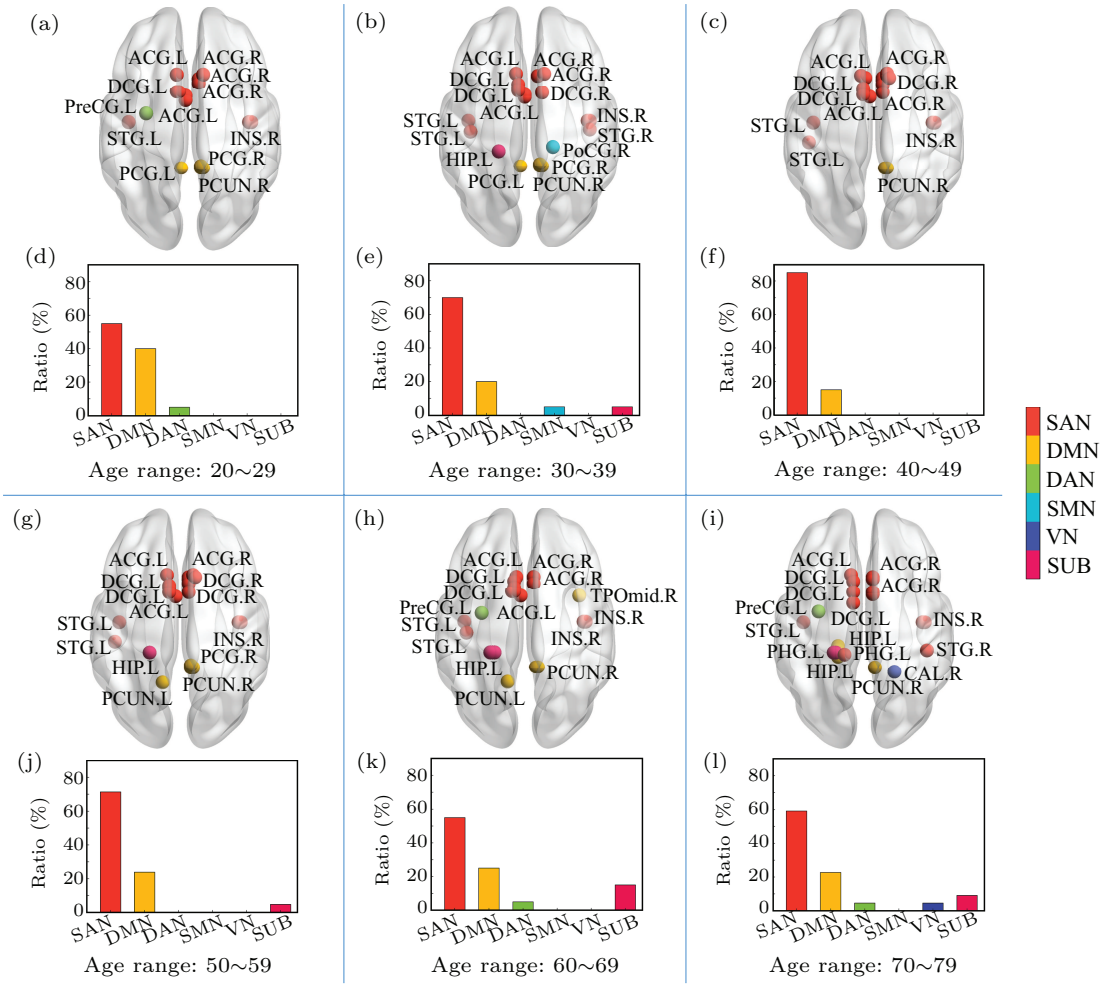


Fig. 5. The distribution of hub nodes as well as the distributions of their assigned brain networks for different age groups (i.e., age ranges 20–29, 30–39, 40–49, 50–59, 60–69 and 70–79 years). In (a)–(c) and (g)–(i), the locations of the hub nodes in different age groups are shown in the axial view and their names are given alongside. Moreover, each hub node is assigned to a corresponding brain network, and the distributions of the ratios for the involved brain networks are shown in (d)–(f) and (j)–(l). To illustrate the results more intuitively, the hub nodes belonging to the same brain network are colored the same as the brain network itself. Additionally, the names of each colored brain network are given in the legend. For hub nodes, ACG = anterior cingulate and paracingulate gyri, DCG = median cingulate and paracingulate gyri, PCG = posterior cingulate gyrus, PreCG = precentral gyrus, STG = superior temporal gyrus, TPOmid=middle temporal gyrus in the temporal pole, PHG = parahippocampal gyrus, PCUN = precuneus, PoCG = postcentral gyrus, INS=insula, CAL = calcarine fissure, HIP = hippocampus, L = left hemisphere, R = right hemisphere. For brain networks, SAN = saliency network, DMN = default mode network, DAN = dorsal attention network, SMN = somatosensory network, VN = visual network, SUB = subcortical network.

4. Discussion

In this study, we explored the pattern of human brain aging using sMRI slices taken from 494 healthy subjects aged 19–80 years. The 2DHVGs were constructed directly based on the pixel values of the slices, and the NNSEs were then extracted to quantify the overall heterogeneities of these graphs. The results suggested that the NNSE of the gray matter increased in early adulthood, reached a peak in the mid-30s, and then decreased with age. By exploring the distribution of hub nodes, we further found that the common hubs in different adult age groups were mostly located in the precuneus, cingulate gyrus, superior temporal gyrus, inferior temporal gyrus, parahippocampal gyrus, insula, precentral gyrus and postcentral gyrus.

Prior studies have demonstrated that the two-dimensional slices and three-dimensional volumes of human brain sMRIs have scale-free characteristics in morphology, which can be measured by fractals and multifractals.[9,18,19] By contrast, our study validated the scale-free characteristics from the perspective of pixel gray values in two-dimensional human brain sMRI slices. Benefiting from the idea of visibility graphs, the inherent characteristics in the original signal can be effectively preserved after network conversion. For a fractal signal, it can be transformed into a scale-free network.[20] According to Luque *et al.*,[21] the adjacency matrix of the HVG can be bidirectionally mapped via its degree sequence, and the degree sequence can cover almost all the information contained in the HVG. Hence, after constructing the 2DHVGs on sMRI slices, we examined their degree distribution information and revealed the intrinsic power law properties in all slices (see Fig. 3). Our findings provide a new perspective for exploring the scale-free characteristics on sMRI data in the human brain.

The heterogeneity of scale-free networks indicates that there are differences in the importance of nodes. In the constructed 2DHVGs, high-degree hub nodes were rare while terminal nodes with small degrees were prevalent. We herein extracted the NNSE values based on their degree feature to measure the overall heterogeneity of 2DHVGs. As a result, the relationship between the NNSEs of the gray matter and age was revealed to exhibit a decreasing trend (Fig. 4). Moreover, NNSEs were generally higher in young people than in the middle-aged and the elderly. For a scale-free network with a power-law distribution of degrees, NNSE can provide insight into the ability of the network to tolerate intrusion.[22] Based on this, it can be inferred that the larger NNSE values in the young group may indicate their more homogeneous network structures, smaller differences in importance between nodes and thus a greater capacity for tolerating intrusion. Intriguingly, similar results can also be obtained by using the resilience index,[23] which is a measure of network resilience to evaluate human brain resilience. Brain resilience refers to the ability of the brain to withstand lesions and maintain a basic level of functionality despite these injuries.[24] Because the most significant functional decreases occur in lesion regions with high centrality[25] this may suggest that the brain is not resilient to attacks on hubs. In young subjects, network structures were more homogeneous, indicating a relatively uniform degree of nodes and fewer super hubs and resulting in a greater ability to tolerate intrusion. Furthermore, Shu *et al.* also reported that the resilience index increased during development and early adulthood, peaked at the age of about 35 years and then decreased with aging.[23] Therefore, the nonlinear decreasing pattern between the resilience index and age was consistent with our findings using NNSE, supporting our hypothesis.

In addition, as shown in Fig. 4, NNSE values showed very little variation across ages (the absolute magnitude is within 0.015). There is a possibility that brain compensation mechanisms might contribute to this. As reported, aging-induced losses and compensation mechanisms might interact during healthy aging.[26] In this process, the brain may exhibit atrophy, which could affect its function. Promisingly, the human brain can compensate for aging losses by recruiting suboptimal brain regions or reorganizing new patterns of activity.[27] When aging occurs in a healthy manner, the compensatory mechanisms in the brain may outweigh the aging loss and the brain may be able to make up for the loss of network connectivity patterns by reorganizing the connections, thus restoring normal brain functioning. Consequently, these two factors might explain why the differences between the NNSE values of healthy old subjects and young subjects were relatively small.

There are several limitations in the current study. First, 2DHVG is limited to some extent in the context of three-dimensional data analysis. As we know, the human brain has a three-dimensional structure. In this sense, a more accurate description of the human brain structure can be achieved by constructing three-dimensional HVGs directly based on volume data. In the current study, we adopted the concept of continuous slices for three-dimensional brain structure analysis, and constructed a series of 2DHVGs on these slices. Although two-dimensional multislice and three-dimensional sMRI sequences are often equally sensitive in capturing effective information,[28] developing a three-dimensional HVG approach may be a promising research direction. Second, the 2DHVGs constructed directly on the pixel signal values are essentially sparse. It is hence imperative to characterize the heterogeneity of sparse networks accurately. Several NSE indices (i.e., degree distribution entropy, SD structure entropy, Wu structure entropy and FB structure entropy) have been proposed to quantify network heterogeneity, and different indices

can measure heterogeneity from different perspectives.[29] In this study, the Wu structure entropy was adopted to measure the heterogeneity of 2DHVGs. Although we achieved some satisfactory results, Wu structure entropy can reflect only local network heterogeneity.[29] Comparatively, FB structure entropy can describe the global topological variation, which might lead to a more accurate identification of network heterogeneity than Wu structure entropy.[29] However, due to the high computational complexity involved in calculating the maximum flow of a network, FB structure entropy cannot currently be directly applied at the voxel level. It is therefore promising to develop a more accurate and efficient structure entropy algorithm that incorporates both global topology variation and local network heterogeneity. In this way, we can promote the further exploitation of the inherent information in the visibility graph.

5. Conclusions

From the novel perspective of gray values in sMRI, this study examined the normal aging pattern of the human brain in healthy individuals from early adulthood to the old age. The 2DHVGs were constructed directly from pixel gray values, and the NNSE was introduced to measure topological heterogeneity. We observed a nonlinear decreasing pattern in NNSE with age from early adulthood to adulthood and old age. Compared with middle-aged and elderly subjects, the larger NNSE values in young subjects were revealed to be associated with the more homogeneous network structures and a greater ability to tolerate intrusion. Furthermore, we also found that the hub nodes of different adult age groups were mainly located in the precuneus, cingulate gyrus, superior temporal gyrus, inferior temporal gyrus, parahippocampal gyrus, insula, precentral gyrus and postcentral gyrus. Our study may contribute to the understanding and exploration of the structural mechanism of brain aging.

Acknowledgements

Project supported by the Natural Science Foundation of Jiangsu Province, China (Grant No. BK20190736); the Young Scientists Fund of the National Natural Science Foundation of China (Grant Nos. 81701346 and 61603198); and Qinglan Team of Universities in Jiangsu Province (Jiangsu Teacher Letter [2020] 10 and Jiangsu Teacher Letter [2021] 11).

References

[1] López-Otín C, Blasco M A, Partridge L, Serrano M and Kroemer G 2013 *Cell* **153** 1194
[2] Cheryl G 2012 *Nature Reviews Neuroscience* **13** 491
[3] Franke K, Bublak P, Hoyer D, Billiet T, Gaser C, Witte O W and Schwab M 2020 *Neuroscience & Biobehavioral Reviews* **117** 142
[4] Bethlehem R A I, Seidlitz J, White S R, *et al*. 2022 *Nature* **604** 525
[5] Takao H, Hayashi N and Ohtomo K 2012 *European Journal of Radiology* **81** 2801
[6] Aycheh H M, Seong J K, Shin J H, Na D L, Kang B, Seo S W and Sohn K A 2018 *Frontiers in Aging Neuroscience* **10** 252
[7] Karolis V R, Callaghan M F, Tseng C E J, Hope T, Weiskopf N, Rees G and Cappelletti M 2019 *Neurobiology of Aging* **79** 83
[8] Takahashi T, Kosaka H, Murata T, Omori M, Narita K, Mitsuya H, Takahashi K, Kimura H and Wada Y 2009 *Psychiatry Research: Neuroimaging* **171** 177
[9] Takahashi T, Murata T, Narita K, Hamada T, Kosaka H, Omori M, Takahashi K, Kimura H, Yoshida H and Wada Y 2006 *NeuroImage* **32** 1158
[10] Iacovacci J and Lacasa L 2018 *IEEE Transactions on Pattern Analysis and Machine Intelligence* **42** 974
[11] Nowak J, Eng R C, Matz T, Waack M, Persson S, Sampathkumar A and Nikoloski Z 2021 *Nat. Commun.* **12** 458
[12] Xiao Q, Pan X, Li X L, Stephen M, Yang H J, Jiang Y, Wang J Y and Zhang Q J 2014 *Chin. Phys. B* **23** 078904
[13] Luque B, Lacasa L, Ballesteros F and Luque J 2009 *Phys. Rev. E* **80** 046103
[14] Wei D, Zhuang K, Ai L, Chen Q and Qiu J 2018 *Scientific Data* **5** 180134
[15] Friston K J, Holmes A P, Worsley K J, Poline J P, Frith C D and Frackowiak R S J 1994 *Human brain mapping* **2** 189
[16] Ashburner J 2007 *NeuroImage* **38** 95
[17] Wu J, Tan Y J, Deng H Z and Zhu D Z 2007 *Systems Engineering - Theory & Practice* **27** 101
[18] King R D, Brown B, Hwang M, Jeon T and George A T 2010 *Neuroimage* **53** 471
[19] Ni H J, Zhou L P, Zeng P, Huang X L, Liu H X and Ning X B 2015 *Chin. Phys. B* **24** 070502
[20] Lacasa L, Luque B, Ballesteros F, Luque J and Nuno J C 2008 *Proc. Natl. Acad. Sci. USA* **105** 4972
[21] Luque B and Lacasa L 2017 *Euro. Phys. J. Spec. Top.* **226** 383
[22] Liu H R, Yin W X, Dong M R and Liu B 2014 *Acta Phys. Sin.* **63** 83 (in Chinese)
[23] Shu P, Zhu H, Jin W, Zhou J, Tong S and Sun J 2021 *IEEE Transactions on Neural Systems and Rehabilitation Engineering* **29** 1756
[24] Pascual-Leone A and Bartres-Faz D 2021 *Annals of Neurology* **90** 336
[25] František V, Murray S, Peter J H, Gregory S, Joana C and Robert L 2015 *NeuroImage* **118** 456
[26] Gonzalez-Escamilla G, Muthuraman M, Chirumamilla V C, Vogt J and Groppa S 2018 *Frontiers in Psychiatry* **9** 601
[27] Cabeza R, Albert M, Belleville S, Craik F I M, Duarte A, Grady C L, Lindenberger U, Nyberg L, Park D C, Reuter-Lorenz P A, Rugg M D, Steffener J and Rajah M N 2018 *Nature Reviews Neuroscience* **19** 701
[28] Johnson G, Wadghiri Y Z and Turnbull D H 1999 *Magnetic Resonance in Medicine* **41** 824
[29] Cai M, Cui Y and Stanley H E 2017 *Scientific Reports* **7** 9340